Appl. Phys. A 88, 443–447 (2007)
DOI: 10.1007/s00339-007-4065-y

Applied Physics A
Materials Science & Processing

M.A. SCHNEIDER[1,2,✉]
P. WAHL[1]
L. VITALI[1]
L. DIEKHÖNER[1,3]
R. VOGELGESANG[1]
K. KERN[1,4]

Local measurement of hot-electron phase-coherence at metal surfaces

[1] Max-Planck-Institut für Festkörperforschung, Heisenbergstr. 1, 70569 Stuttgart, Germany
[2] Lehrstuhl für Festkörperphysik, Universität Erlangen, Staudtstr. 7, 91058 Erlangen, Germany
[3] Aalborg Universitet, Institut for Fysik og Nanoteknologi, Skjernvej 4A, 9220 Aalborg, Denmark
[4] Institut de Physique des Nanostructures, Ecole Polytechnique Fédérale de Lausanne, 1015 Lausanne, Switzerland

Received: 27 July 2006/Accepted: 4 April 2007
Published online: 9 June 2007 •

ABSTRACT We use scanning tunneling microscopy and spectroscopy to study the energy dependence of hot-electron scattering processes on metal surfaces via the determination of the energy-dependent phase-coherence length. From this an electron lifetime can be determined, which in the case of electrons in the surface state of Ag(111) and in the case of the $n = 1$ image-potential state on Cu(100) shows good agreement with theoretical modeling and other experimental data. The method is based on the quantitative analysis of electron interference patterns. A theoretical analysis shows that the phase-coherence length can be determined in confining nanostructures of a characteristic length scale smaller than the phase-coherence length.

PACS 73.20.At; 73.50.Gr; 72.10.Fk; 68.37.Ef

1 Introduction

The lifetime of an electronic excitation at surfaces is of great interest in many areas of physics and chemistry. A sufficiently long lifetime is needed to e.g., transfer energy and charge from the excitation and thereby trigger other dynamical processes. The phase coherence of an electron is limited by inelastic electron–electron and quasi-elastic electron–phonon scattering. Hence, the dephasing time at metal surfaces corresponds to the energy relaxation time measured e.g., by photoelectron spectroscopy [1]. There are three main motivations to study lifetime effects by scanning tunneling microscopy (STM). Firstly, by STM one obtains an atomic scale information about the defect configuration (at the surface) of the sample and hence one can characterize the defect contribution to the lifetime. Secondly, scanning tunneling spectroscopy (STS) allows one to study occupied and unoccupied electronic states with a high energy resolution and with a single method. Thirdly, STM can access nanostructures at surfaces and the influence of size and shape on the lifetime of electrons can be studied.

There is a great interest to understand the dynamics of electrons in two-dimensional surface and image-potential states. As has been shown by Gauyacq and co-workers the properties of the surface band structure are a decisive ingredient for understanding the lifetime of excited states at e.g., alkali adsorbates but also for understanding the interaction of charged ions with metal surfaces [2, 3]. In the case of noble metal (111) and (100) surfaces the appearance of directional band gaps hinders resonant charge transfer from an adsorbate to the substrate which is most effective for states with small momentum transfer parallel to the surface. Surface states and image-potential states fill these gaps. Their lifetimes gain importance in the relaxation of excited adsorbate states. If the relevant processes could be steered one would gain "quantum control" of adsorbate motion and possibly reactivity on metal surfaces [4]. To this end the modification of the surface by epitaxy, surface alloying, or by nanostructuring is a promising tool and its effect on the electronic lifetime need to be studied. Surface and image-potential states are model states to probe quantum coherence in two-dimensional and – if confined – even in one- or zero-dimensional systems. Due to their special nature at the surface they exhibit reasonably long lifetimes so that decay mechanisms within the low-dimensional quantum systems can be studied in metallic systems. Here we apply the method of using an STM to determine the electronic phase-coherence length to surface and image-potential states and discuss the applicability to electrons in confining nanostructures.

2 Experimental

Single crystal surfaces were prepared by sputtering and annealing cycles in ultra-high vacuum (base pressure 1×10^{-10} mbar). The samples were transferred in situ to an STM working at 6 K.

The idea followed here to gain access to electron lifetimes by STM and to study the lifetime on a local scale is based on the observation of electron interference patterns. Electrons scattered at defects interfere with themselves. By this a spatial modulation of the LDOS is created. Such interference patterns are observed in a variety of systems exhibiting surface states [5–9] but can also be observed for electrons injected into image-potential states with an excess-energy close to (or in the case of STM: above) the vacuum level of the crystal [10]. These patterns not only contain the dispersion $E(k)$ of the state via the energy-dependent wave length of the oscilla-

✉ Fax: +49 9131 852 8400,
E-mail: alexander.schneider@physik.uni-erlangen.de

tions but also the phase-coherent length of the electrons which is responsible for a loss of oscillation amplitude with distance from the scatterer [7].

Consequently, spatial $\mathrm{d}I/\mathrm{d}V$ maps as function of tunneling bias were taken using a lock-in technique with a 4.5 kHz modulation of the sample voltage of the order of 10% of the difference between applied dc bias and the voltage at which the onset of the state probed appears. The loss of coherence leads to a spatial decay of the contrast of the interference pattern. Careful separation of other effects like the energy broadening introduced by the modulation technique but also of geometrical effects allows a quantitative determination of the phase-coherence length of the electrons at the relevant energy [7]. The wave pattern caused by a scatterer is fitted incorporating a probability of the decay of coherent wave amplitude. To keep the analysis simple, the scattering pattern at a straight step edge was evaluated [7, 10, 11]. Avoiding further scatterers nearby guarantees the determination of a phase-coherence length in the clean limit. However, the consideration of further scatterers poses no problem and has been demonstrated [12]. The phase-coherence approach measures the decay of coherence caused by the propagation of the electrons at the clean surface. The amplitude absorbed by the scatterer will diminish the intensity found in the interference pattern independent of distance from the scatterer. Further implications will be discussed below.

To compare different theoretical and experimental results the measured phase-coherence length needs to be converted to a lifetime. It was pointed out by Crampin et al. [13] that the generally used lifetimes correspond to phase-coherence lengths defined as the decay of the wave-function squared contrary to our original definition as the decay of the wave-function [7]. Therefore, we use in the following the spatial variation of the energy dependent electron LDOS at a step-edge in a two-dimensional electron gas given by:

$$\varrho(x, E) \propto L_0\left(1 - r\mathrm{e}^{-x/L_\varphi(E)} J_0(2k_\parallel(E)x)\right). \tag{1}$$

Here x is the spatial distance from the step edge, E is the energy of the interfering states, L_0 is the (constant) density of states, r is the reflectivity of the step edge, $k_\parallel(E)$ is the wave vector in the surface plane, and $L_\varphi(E)$ is the phase-coherence length. L_φ differs from the previous definition by a factor of two, i.e., the previously obtained phase-coherence lengths were too large. The measured $\mathrm{d}I/\mathrm{d}V$ signal is taken to be proportional to $\varrho(x, E)$. In the graphs the phase-coherence lengths are converted into a hypothetical state line-width $\Gamma(E)$ by use of the relation:

$$\Gamma(E) = \frac{\hbar}{\tau_\varphi(E)}; \qquad \tau_\varphi(E) = \frac{L_\varphi(E)}{v(E)}, \tag{2}$$

where τ_φ is the phase-coherence time and $v(E)$ is the group velocity of the electrons with energy E. $v(E)$ is obtained experimentally from the dispersion relation $E(k)$ via:

$$v(E) = \frac{1}{\hbar}\frac{\partial E}{\partial k} = \frac{\hbar k(E)}{m^*} \tag{3}$$

with the effective mass m^*.

3 Hot-electron lifetime at noble metal surfaces: Ag(111)

The theory of inelastic lifetimes of electrons at metal surfaces has been developed and reviewed by Echenique and co-workers [1, 14]. Looking at electron–electron interaction first, to calculate the lifetime of hot electrons in these surface states one needs the interaction potential, the available initial and final states and their density. The relaxation process evolves via the creation of an electron–hole pair that takes up energy and momentum from the hot electron. From Fermi's golden rule one expects that the scattering rate is enhanced if initial and final states have a large spatial overlap, if there is a high density of final states, and if the interaction potential is large, i.e., screening between scattering partners is small [1]. In the case of electron–electron scattering the coupling within the many-body system is approximated by the screened Coulomb interaction between scattering partners. In a bounded electron system this interaction becomes a function of position and is peaked at the surface since the decay of electronic states at surfaces into the vacuum reduces the screening between electrons located at the surface. In consequence, calculated scattering rates depend delicately on the electronic wave functions. Since the computational effort to use fully three-dimensional models for obtaining scattering rates at surfaces is still prohibitive, relatively simple one-dimensional models are used, that reproduce the experimentally found eigenenergies of surface and image-potential states and the states at the projected bulk band-gap [11, 14].

With this simplification one can obtain calculated scattering rates that agree very well with those from experiments and also allow to illustrate the relative importance of different scattering channels [1]. The measurement of

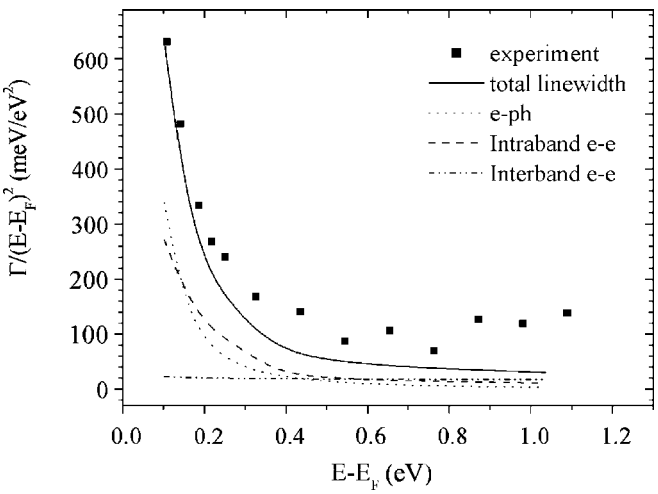

FIGURE 1 The inverse lifetime expressed as a linewidth $\Gamma = \hbar/\tau_\varphi$ of surface-state electrons on Ag(111). Shown are experimental values obtained by STM (*symbols*) and calculated linewidths that show the relative importance of different scattering channels. Γ is scaled with $1/(E - E_\mathrm{F})^2$. Hence the interband scattering (scattering rate $\propto (E - E_\mathrm{F})^2$) appears as a flat line. Phonons introduce an energy independent broadening of 3.5 meV, hence the phonon contribution in $\Gamma/(E - E_\mathrm{F})^2$ increases for low energies. So does the intraband contribution since below 0.4 eV the surface state is no longer a surface resonance and gains importance. The total calculated linewidth is given by the sum of the individual contributions. Corrected figure from [11]

energy dependent hot-electron lifetimes allowed a detailed comparison between experiment and theory in the case of surface-state electrons on Ag(111) [7, 11]. Here we correct the data for the above mentioned factor of two. Figure 1 shows good agreement between experiment and calculations especially for the important regime of low excess energies. This comparison leads to the conclusion that the lifetime is dominated by intraband scattering in the energy regime between 100 and 400 meV. For higher energies the STM data show slightly broadened linewidths compared to the calculation which could be due to the assumptions made in the model [11].

4 Phase coherence of electrons in image-potential states

Similarly the energy dependence of the coherence length of electrons in image-potential states on Cu(100) was measured [10]. For these states one needs to consider the special situation encountered in the electric field of the STM junction. Since the radius of curvature of the tip is likely to be of the order of 10–50 nm a constant electric field in the junction is assumed. This electric field not only shifts the energetic positions of the image-potential states relative to the Cu(100) gap at the X-point of the bulk Brillouin zone but also enhances the penetration of the state into the bulk crystal.

The phase-coherence length as measured by STM is found to stay approximately constant in the energy window $E_0 + 0.2\,\mathrm{eV} < E < E_0 + 0.5\,\mathrm{eV}$ from which a linearly increasing $\Gamma(E)$ was deduced. The comparison with 2PPE data [15] shows that the STM derived linewidth is roughly twice that of the linewidth measured by 2PPE (Fig. 2). To compare the Stark-shifted with the undisturbed situation it is not enough to consider the energetic position of the state within the bulk band gap. This approach was successful to compare the properties of image-potential states at different *d*-metal surfaces [17]. Similar to the situation of the electrons in the surface state of Ag(111) the decay of the image-potential state

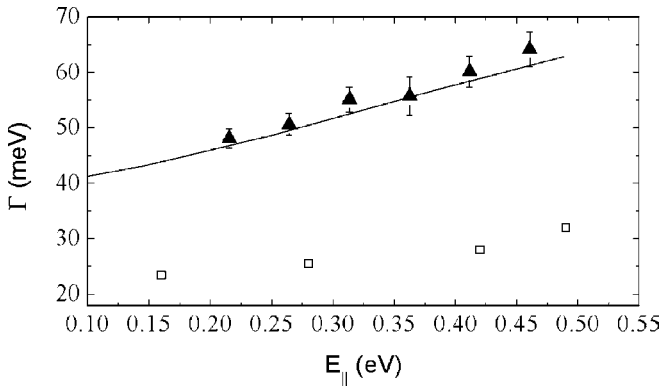

FIGURE 2 The inverse lifetime expressed as a linewidth $\Gamma = \hbar/\tau_\varphi$ of the $n = 1$ image-potential state on Cu(100) as function of kinetic energy parallel to the surface $E_\parallel = E - E_1$, where E is the total energy of the injected electron and E_1 is the binding energy of the $n = 1$ state. *Solid symbols* are the corrected measured values from [10], *open symbols* are the values measured by two-photon photoemission (2PPE) [15]. The *solid line* is the theoretical calculation given in [15] modified to take into account the effect of the Stark shift in the STM junction (see text). The Stark shift enhances the interband scattering between image-potential and bulk electrons [16]

population is given by interband scattering into the bulk and to a considerable degree by intraband scattering for electrons with higher kinetic energy $E_\parallel = E - E_1$, where E is the total energy of the electron and E_1 the onset energy of the $n = 1$ state [15]. As outlined above the rate of interband scattering is proportional to the overlap of initial and final states and can be estimated by the bulk penetration p of the state at the crystal surface that can be defined as [14]:

$$p = \int_{\mathrm{bulk}} \psi(z)^* \psi(z)\,\mathrm{d}z\,, \tag{4}$$

where $\psi(z)$ is the image-potential wave function. A model potential was used to obtain the image-potential wave functions in the presence of the STM tip [10]. For those states p increases by a factor 2.2 for the $n = 1$ state. In consequence, one expects an enhanced interband scattering rate. On the other hand, the intraband contribution should be unchanged since it depends on the overlap of image-potential wave functions for different $E_\parallel$. These are all equally affected by the tip potential. The interband and intraband contributions were calculated by Berthold et al. [15] and showed agreement with their 2PPE data. If one multiplies the interband contribution by 2.2 and keeps the same intraband contribution as [15] good agreement with the STM-linewidths is obtained [16]. It is apparent that the same physical mechanisms cause the decay of the interference patterns in STM as well as the decay of population of the image-potential states in 2PPE (Fig. 2). A rigorous theoretical treatment in the framework of the GW approximation supports this analysis [18].

5 Discussion

In conclusion one can note that electron lifetimes of surface and image-potential states extracted from local measurements of the phase-coherence length agree well with theoretical modelling and also with available 2PPE data. The same is true for the linewidths of hole excitations as measured by STS and PES [19]. At first sight this agreement is surprising since for a long time the residual difference between PES linewidths and theoretical calculations was blamed on defect scattering. However, improvements in the energetic resolution of PES experiments better control of the amount of adsorbates on the surfaces reduced experimental linewidths over the last decade and lead to a consistency between PES, theory and local STS measurements on defect free surfaces [20]. Terrace widths of the order of 100 nm seem to be large enough to not influence the life-time of electrons in surface or image-potential states. Linewidth broadening of surface states is caused by defects or disorder on a nanometer length scale as seen in the experiments of Theilmann et al. [21] in the case of surface states or Reuß et al. [22] and Boger et al. [23] in the case of image-potential states.

STS can, in principle, be used to study the linewidth of energetically well localized states at metal surfaces [19, 24–26]. If applied to states in electron resonators, e.g., islands or adatom structures created by atomic manipulation [24, 25], the linewidth depends on the properties of the confining potential as well as on the scattering processes discussed in this paper [27]. Thus the question arises how the border of a nanostructure and its size may limit the reliable determination of

L_φ of electrons of the undisturbed surface, particularly if the coherence length is larger than the spatial extent of the resonator. Provided one has a suitable model for scattering at the confining border, its effect on the LDOS pattern can be separated from processes determining L_φ as both introduce distinctly different effects on the LDOS pattern. The loss of coherence during propagation may be described by a modification of the free space Green function to include an additional exponential decay with propagation distance.

In the following analysis, we are concerned with the case of coherence lengths L_φ larger than the size of the resonator given by some characteristic length R. The aim is to provide a measure for the relation between the error in L_φ and the size of the resonator. We assume that other systematic sources of error, as e.g., the finite voltage modulation used in the experiment have been treated in addition [7]. The difference between two standing wave patterns with L_φ and $L_\varphi + \Delta L_\varphi$ may be obscured by noise, i.e., they will be indistinguishable. Correspondingly, we expect to be able to determine L_φ by means of some regression analysis only with a certain accuracy $\sigma_\varphi = |\Delta L_\varphi|/L_\varphi$. Clearly, this accuracy depends on the relative noise $\tilde{N}$ that enters the measurement, which can be estimated directly from the data as the statistical noise N of a single measurement relative to the contrast in the interference pattern. We now derive a simple relation which allows a rough estimate of the phase coherence length relative to the resonator size, $\tilde{L}_\varphi = L_\varphi/R$, which can just be determined with an accuracy σ_φ at a given noise level $\tilde{N}$.

The LDOS is the imaginary part of the full Green function, which is obtained by an evaluation of the Born series. Modelling resonators as an array of many interacting point scatterers, allows the full Born series to be evaluated algebraically [28]. Here, we consider the first order Born approximation term, which is essentially the interference from all point scatterers making up the resonator border in the absence of any multi-scattering events. These provide the finer details of the experimental LDOS pattern but the qualitative trends we find below will be preserved.

In the first-order Born approximation, the influence of the phase-coherence length can be evaluated with the Green function of isotropic space. Neglecting multiple scattering at the confining boundary is appropriate due to the "lossy" nature of scattering at the boundary [29]. The spatial LDOS variation at a fixed energy due to a single scatterer in the border resembles a damped spherical oscillation in space

$$\varrho(r, \lambda, L_\varphi) = \xi \mathrm{e}^{-r/L_\varphi} \frac{\sin(2\pi r/\lambda + \delta)}{r^\nu} \tag{5}$$

with wavelength λ and phase shift δ. The amplitude factor ξ contains the reflectivity of the single scattering event. The envelop function $\varrho_0(r) = \xi \exp(-r/L_\varphi)/r^\nu$ incorporates the exponential decay with propagation distance. The exponent ν depends on the dimensionality of the system, making our argument also applicable to one- and three-dimensional systems. For two-dimensional systems $\nu = 1/2$, $\delta = \pi/4$ and (5) is the far-field approximation of (1).

We measure the corresponding LDOS variation along a certain radial interval R, which we associate with a characteristic experimental length scale, e.g., the radius of a circular resonator. Given a position-independent noise N, one has to ask how precise a value can be extracted for the coherence length from the given data. Certainly we can reject the result L'_φ of some non-linear fitting procedure from the proper length L_φ if for some data points at r the difference between the waves exceeds the noise, $|\varrho(r, \lambda, L_\varphi) - \varrho(r, \lambda, L'_\varphi)| > N$ (Fig. 3a). Most likely this occurs at the peaks of the LDOS pattern. For a sufficient density of peaks (i.e., the observed interval contains several wavelengths of oscillation), a good measure of an acceptable fit is the spread in the envelop function being contained within the noise band, $|\varrho_0(r, \lambda, L_\varphi) - \varrho_0(r, \lambda, L'_\varphi)| < N$ (Fig. 3b). In the delicate case of long coherence lengths $L_\varphi > R$, this results in

$$\xi \left| \frac{\mathrm{e}^{-R/L'_\varphi}}{R^\nu} - \frac{\mathrm{e}^{-R/L_\varphi}}{R^\nu} \right| \leq N\,. \tag{6}$$

We define the relative noise as $\tilde{N} = N/\varrho_0(R)$. With this, the largest coherence length $\tilde{L}_\varphi = L_\varphi/R$ relative to the resonator size that can be determined with an accuracy σ_φ is given by

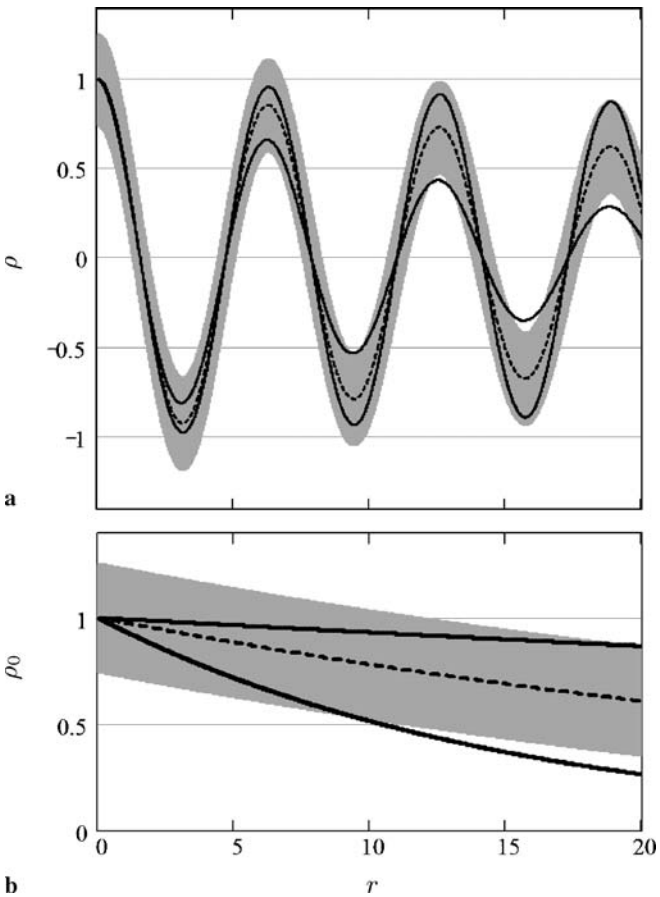

FIGURE 3 One-dimensional illustration of the range of acceptable fits for the phase-coherence length L_φ to a given noisy measurement of LDOS variations over an interval of $R = 20$ length units. (**a**) The measured spatial LDOS variation ϱ is assumed to be contained within the gray noise band (25% of the maximum signal). The *dotted line* corresponds to a signal with $L_\varphi = 40$, i.e. twice the displayed interval. The *solid curves* indicate two possible outcomes of a fitting procedure. The barely acceptable fit with $L_\varphi = 140$ is contained within the noise band, while a fit with $L_\varphi = 15$ would be rejected as it exceeds the noise band. (**b**) The amplitude envelops of the oscillatory functions in (**a**)

$$\tilde{L}_\varphi = \frac{1}{\ln(1+\tilde{N})}\,\frac{1}{1+\sigma_\varphi^{-1}}\,. \tag{7}$$

For $\tilde{N} \ll 100\%$ and $|\Delta L_\varphi| \ll L_\varphi$ applicable to actual experimental conditions this turns into the fairly simple relation $\sigma_\varphi = \tilde{L}_\varphi \tilde{N}$, which provides a convenient estimation of the achievable results. Evidently, longer coherence lengths can be determined only at the expense of either relaxed accuracy σ_φ or improved sensitivity $\tilde{N}$. On the one hand $\tilde{N}$ depends on the experimental measurement noise which can be reduced by increasing the number of data points taken or the accuracy of each point (through slower measurements). However, the achievable gain in accuracy is practically limited due to the increased time needed to conduct the experiment.

On the other hand, $\tilde{N}$ depends on the resonator and its quality factor via the considerable variation of $\varrho_0(R)$ with energy at resonance. A high-quality resonator in resonance results in the largest modulation amplitudes for the standing wave patterns and thus the best fit results for $\tilde{L}_\varphi$.

Figure 4 shows that for a good sensitivity, i.e., low measurement noise $\tilde{N}$ toward the spatial variation of the LDOS signal a phase-coherence larger than the actual size of the resonator can be detected. For currently available low-temperature STMs and for resonators formed by adatom corals or nanometer sized islands we estimate $0.01 < \tilde{N} < 0.1$. Thus coherence lengths of up to 10 times the resonator size may be measured with reasonable accuracy. Compared to the analysis of resonator linewidths [27] the L_φ-method is slightly more favorable to detect electron–electron interaction in small nanostructures. Our analysis is applicable to the work of Braun and Rieder [12]. For the data taken close to the Fermi energy, the determination of L_φ seems not reliable as the size of the resonator is more than ten times smaller than L_φ. The observed short period variation of measured phase-coherence length with energy could be due to the influence of the resonances on $\tilde{N}$ where a measurement taken off-resonance implies a larger $\tilde{N}$.

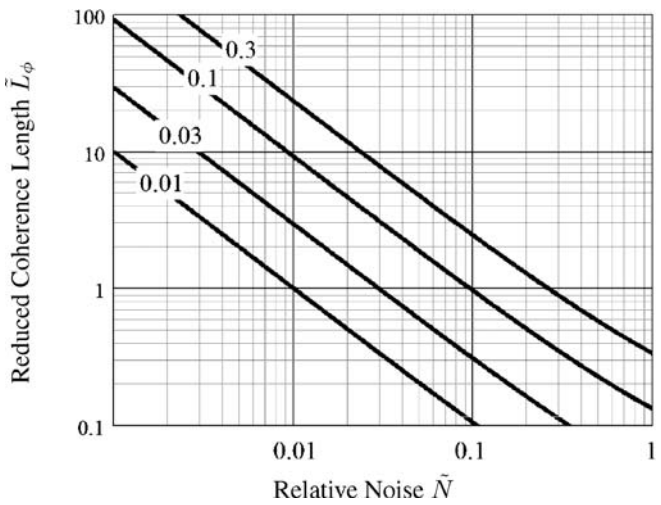

FIGURE 4 The prediction according to (7) for the maximum reduced phase-coherence length L_φ/R obtainable for different degrees of desired accuracy σ_φ, plotted as functions of the relative measurement noise $\tilde{N}$. For instance, for an accuracy of $\sigma_\varphi = 10\%$ and a relative noise of less than $\tilde{N} = 5\%$, it is possible to determine coherence lengths of up to twice the resonator size

6 Conclusions

Low temperature STS measurements were used to determine the phase-coherence length and thereby the life-time of electrons in two-dimensional states at metal surfaces. In the case of hot surface-state electrons on Ag(111) a comparison with life-time calculation explains the observed energy dependence by the relative importance of inter- and intra-band electron–electron scattering and electron–phonon scattering. In the case of electrons in the image-potential $n = 1$ state of Cu(100) the electric field of the STM tip enhances the contribution of inter-band electron–electron scattering. Taking this into account demonstrates a good agreement between local and non-local determinations of electron life-times in this specific case. An analysis of the detection limit of the method indicates that the phase-coherence length L_φ may also be extracted from the local density of states in nanostructures of size comparable to or slightly smaller than L_φ.

REFERENCES

1 P. Echenique, R. Berndt, E. Chulkov, T. Fauster, A. Goldmann, U. Höfer, Surf. Sci. Rep. **52**, 219 (2004)
2 A. Borisov, J. Gauyacq, A. Kazansky, E. Chulkov, V. Silkin, P. Echenique, Phys. Rev. Lett. **86**, 488 (2001)
3 T. Hecht, H. Winter, A. Borisov, J. Gauyacq, A. Kazansky, Phys. Rev. Lett. **84**, 2517 (2000)
4 H. Petek, H. Nagano, M.J. Weida, S. Ogawa, J. Phys. Chem. A **104**, 10234 (2000)
5 M.F. Crommie, C.P. Lutz, D.M. Eigler, Nature **363**, 524 (1993)
6 B.G. Briner, P. Hofmann, M. Doering, H.-P. Rust, E.W. Plummer, Phys. Rev. B **58**, 13931 (1998)
7 L. Bürgi, O. Jeandupeux, H. Brune, K. Kern, Phys. Rev. Lett. **82**, 4516 (1999)
8 N. Sato, S. Takeda, T. Nagao, S. Hasegawa, Phys. Rev. B **59**, 2035 (1999)
9 L. Diekhöner, M. Schneider, A. Baranov, V. Stepanyuk, K. Kern, Phys. Rev. Lett. **90**, 236801 (2003)
10 P. Wahl, M. Schneider, L. Diekhöner, R. Vogelgesang, K. Kern, Phys. Rev. Lett. **91**, 106802 (2003)
11 L. Vitali, P. Wahl, M. Schneider, K. Kern, V. Silkin, E. Chulkov, P. Echenique, Surf. Sci. **523**, L47 (2003)
12 K.-F. Braun, K. Rieder, Phys. Rev. Lett. **88**, 096801 (2002)
13 S. Crampin, J. Kröger, H. Jensen, R. Berndt, Phys. Rev. Lett. **95**, 029701 (2005)
14 P. Echenique, J. Pitarke, E. Chulkov, A. Rubio, Chem. Phys. **251**, 1 (2000)
15 W. Berthold, U. Höfer, P. Feulner, E. Chulkov, V. Silkin, P. Echenique, Phys. Rev. Lett. **88**, 056805 (2002)
16 P. Wahl, M. Schneider, L. Diekhöner, R. Vogelgesang, K. Kern, Phys. Rev. Lett. **95**, 029702 (2005)
17 H. Rhie, S. Link, H. Dürr, W. Eberhardt, N. Smith, Phys. Rev. B **68**, 033410 (2003)
18 S. Crampin, Phys. Rev. Lett. **95**, 046801 (2005)
19 J. Kliewer, R. Berndt, E.V. Chulkov, V.M. Silkin, P.M. Echenique, S. Crampin, Science **288**, 1399 (2000)
20 F. Reinert, G. Nicolay, S. Schmidt, D. Ehm, S. Hüfner, Phys. Rev. B **63**, 115415 (2001)
21 F. Theilmann, R. Matzdorf, A. Goldmann, Surf. Sci. **420**, 37 (1999)
22 C. Reuß, I. Shumay, U. Thomann, M. Kutschera, M. Weinelt, T. Fauster, U. Höfer, Phys. Rev. Lett. **82**, 153 (1999)
23 K. Boger, M. Weinelt, T. Fauster, Phys. Rev. Lett. **92**, 126803 (2004)
24 J. Kliewer, R. Berndt, S. Crampin, New J. Phys. **3**, 22 (2001)
25 H. Jensen, J. Kroeger, R. Berndt, S. Crampin, Phys. Rev. B **71**, 155417 (2005)
26 A. Bauer, A. Mühlig, D. Wegner, G. Kaindl, Phys. Rev. B **65**, 075421 (2002)
27 S. Crampin, H. Jensen, J. Kröger, L. Limot, R. Berndt, Phys. Rev. B **72**, 035443 (2005)
28 E.J. Heller, M.F. Crommie, C.P. Lutz, D.M. Eigler, Nature **389**, 464 (1994)
29 L. Bürgi, O. Jeandupeux, A. Hirstein, H. Brune, K. Kern, Phys. Rev. Lett. **81**, 5370 (1998)